Journal of Magnetism and Magnetic Materials 540 (2021) 168481

Contents lists available at ScienceDirect

Journal of Magnetism and Magnetic Materials

journal homepage: www.elsevier.com/locate/jmmm

The key role of reaction temperature on a polyol synthesis of water-dispersible iron oxide nanoparticles

Pohlee Cheah [a], Jing Qu [a], Yu Li [b], Dongmei Cao [b], Xianchun Zhu [a], Yongfeng Zhao [a,*]

[a] Department of Chemistry, Physics and Atmospheric Science, Jackson State University, Jackson, MS 39217, USA
[b] Material Characterization Center, Louisiana State University, Baton Rouge, LA 70803, USA

ARTICLE INFO

Keywords:
Iron oxide nanoparticle
Temperature
Polyols
Water soluble
Magnetic property
Thermal decomposition

ABSTRACT

The controlled synthesis of water-dispersible iron oxide nanoparticles is essential for biomedical application. For the continuous growth of iron oxide nanoparticles in polyols, it is still unclear how the temperature will affect the controlled synthesis of water-dispersible iron oxide nanoparticles. This work studies the role of reaction temperature on the continuous growth of water-dispersible iron oxide nanoparticles in diethylene glycol (DEG). At the temperature of 235 °C and below, the nanoparticle size increases with the increase of temperature. These nanoparticles are highly water dispersible. Interestingly, with the further increase of temperature to the boiling point of DEG (245 °C), precipitations are produced during the reaction. The resulted nanoparticles are not stable in an aqueous solution anymore. X-ray Photoelectron Spectroscopy (XPS) analysis is employed to study the surface changes of nanoparticles prepared at different temperatures. The size, crystal structure, and magnetic properties of these nanoparticles are characterized by TEM, DLS, XRD, XPS, FTIR, and SQUID magnetometry. The crystallite sizes from XRD match very well with those by TEM. The nanoparticles consist of a single-grain domain. The crystal structure of the nanoparticles exhibits a magnetite phase. The magnetization properties are studied for the nanoparticle synthesized at different reaction temperatures. The water-dispersible nanoparticles can be used for potential magnetic resonance imaging which is indicated by their transverse (r_2) and longitudinal relaxivities (r_1). The relaxivity properties are consistent with the size of nanoparticles prepared at various temperatures.

1. Introduction

Magnetic iron oxide nanoparticles emerge as a prominent materials due to their tunable magnetic properties and excellent biocompatibility [1,2]. Their broad applications in biomedicine include magnetic separation, drug delivery, biomedical imaging, and magnetic hyperthermia therapy [3–5]. The physicochemical properties such as size and water solubility of iron oxide nanoparticles are crucial in realizing these end applications. To date, several synthesis methods for iron oxide nanoparticles have been reported, such as coprecipitation [6,7], sonochemistry [8–10], microemulsion [11], hydrothermal [12–14], and polyol method [15,16]. It is the ultimate goal and remains a challenge to synthesize iron oxide nanoparticles with precisely controlled size and high water solubility.

Thermal decomposition of iron precursors in organic solvents with high boiling points has been the most widely used method to synthesize iron oxide nanoparticles with well-controlled sizes, high crystallinity, and narrow size distributions [17–18]. The disadvantage is that these nanoparticles required extra treatment or a post-synthesis ligand exchange process to acquire water dispersity. The surface modification process is proven to be time-consuming and sophisticated in practice [19–20]. Recently, thermal decomposition of iron precursor in polyol solvents has been receiving great attention due to the facile strategy in synthesizing water-soluble superparamagnetic iron oxide nanoparticles in one step [21–24]. The choice of solvents includes ethylene glycol (EG), diethylene glycol (DEG), triethylene glycol (TREG), tetraethylene glycol (TEG), or short-chain polyethylene glycol.

As an important reaction parameter, the reaction temperature has been reported to affect the size of nanoparticles. In general, the size of nanoparticles increases with an increase in reaction temperature due to the high growth rate [25–29]. A majority of these studies on temperature were conducted on the synthesis of iron oxide nanoparticles in organic solvents system [30,31] or with the involvement of surface coating materials [25,29]. A few studies were conducted to study the

* Corresponding author.
E-mail address: yongfeng.zhao@jsums.edu (Y. Zhao).

https://doi.org/10.1016/j.jmmm.2021.168481
Received 24 May 2021; Received in revised form 24 August 2021; Accepted 25 August 2021
Available online 31 August 2021

effect of temperature on the thermal decomposition method in polyols systems.

Wan et al. [15] studied the thermal decomposition of $Fe(acac)_3$ in different polyols solvents. They found that iron oxide nanoparticles would aggregate, and size distribution was broad when the reaction was conducted in DEG. The synthesis in TREG would lead to non-aggregated monodisperse nanoparticles. Thanh et al. [32] reported the iron oxide nanoparticles with low polydispersity through a simple polyols synthesis in high pressure and high temperature. The study confirmed that solvents were critical to obtain high-quality nanoparticles. However, these reactions were carried out in various solvents with different boiling points. It was not possible to separate the effect of solvents themselves from the reaction temperatures [15]. The conclusions from the studies in polyols systems were rather comprehensive and lack of reproducibility with a few observed aggregation or instability of nanoparticles product.

We recently reported a continuous growth strategy to synthesize iron oxide nanoparticles in DEG [21]. The strategy is proven to be facile to produce highly water-dispersible nanoparticles. Nevertheless, the study of temperature on the synthesis of iron oxide nanoparticles was not realized in DEG.

In this work, we will further study the effect of the reaction temperatures on the continuous growth strategy and the water stability of the nanoparticles. We find that reaction temperature plays a key role in controlling the size of iron oxide nanoparticles in DEG and affects the water solubility as well. It has not been reported that the reaction temperature could affect the stability of iron oxide nanoparticles in polyol synthesis.

2. Experimental section

2.1. Chemicals and materials

Iron (III) acetylacetonate ($Fe(acac)_3$) $\geq$ 99.9 %, diethylene glycols (DEG), were purchased from Sigma-Aldrich (St. Louis, USA). All chemicals were used without further purification, Gibco™ phosphate-buffered saline (PBS) tablets, Milli-Q water was used in this study.

2.2. Methods

The synthesis of iron oxide nanoparticles follows our previous study [21]. Different reaction temperatures were studied, 190, 220, 235 °C and reflux temperature (245 °C). Typically, $Fe(acac)_3$ (88 mg, 0.25 mmol) was mixed and stirred with DEG (2.5 mL, 0.1 mmol Fe/mL) in a three-necked flask under argon gas exchange to obtain solution A. In another flask, $Fe(acac)_3$ (211 mg, 0.6 mmol) was mixed with DEG (6 mL, 0.1 mmol Fe/mL), and the mixture was stirred under argon to obtain solution B. Both solutions were heated to 120 °C for an hour. Solution B was kept at 70 °C for later use. Solution A was further heated slowly (heating rate of 2.5 °C/min) to the desired reaction temperature for 2 h as the first growth. After that, solution B (2.5 mL, 0.25 mmol) was subsequently added to react for another 2 h as the second growth. The addition of solution B continued and react for another 2 h as the third growth. The procedure was summarized as Scheme 1.

2.3. Characterizations

The core size of the nanoparticles was characterized by using a transmission electron microscope (TEM) JEOL JEM 1011. The dilute water dispersion of nanoparticles was cast on an ultrathin 150-mesh carbon-coated grid and allowed to dry at room temperature. The size analysis from TEM images was performed using ImageJ software (Version 1.52a) by first applying the smoothing filter and collecting the measurement of 100 particles. The data was further fitted by normalized distribution using OriginPro 2018. The X-ray diffractograms were collected under a Rigaku MiniFlex 600 X-ray diffractometer (40 kV, 15 mA) using Cu Kβ radiation ($\lambda = 0.154$ nm). The scan degree was from

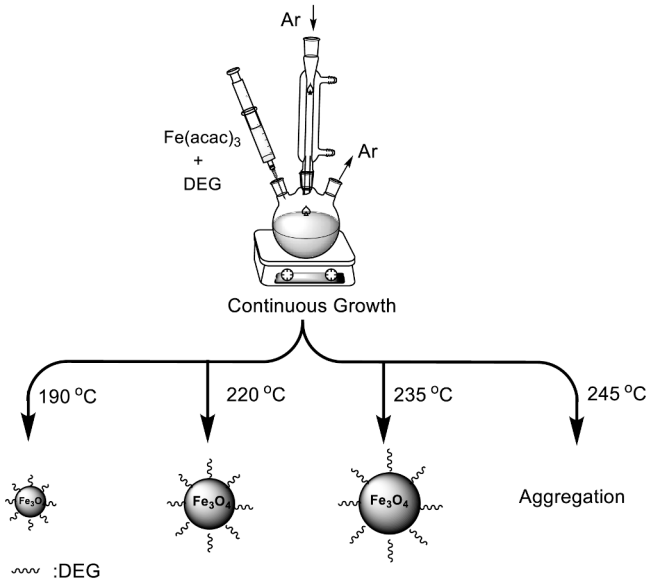

Scheme 1. Procedure for the continuous growth of water-dispersible iron oxide nanoparticles at 190 °C, 220 °C, 235 °C, and reflux temperature (245 °C).

10° to 80°, step degree of 0.01 at the rate of 1° /min. Based on the strongest peak of (311), the crystal sizes of iron oxide nanoparticles were calculated according to the Debye-Scherrer equation: $D_{hkl} = k\,\lambda/\beta \cos\theta$. Here D_{hkl} is crystallite size parallel to the (*hkl*) plane, k is a constant of typical 0.89, λ is the wavelength of the X-ray source, β is full width at half maximum (FWHM) of diffraction peak, and θ is the angle of diffraction peak. After the purification, nanoparticles were dispersed in Milli-Q water, and 1× phosphate buffer saline (PBS) solution, and pictures were taken on certain days to observe the stability over time. The hydrodynamic size was studied with dynamic light scattering (NanoZS, Malvern, Worcestershire, UK). The magnetic properties were performed by the superconducting quantum interference device (SQUID, Quantum Design, MPMS XL). Field cooled (FC) and zero field cooled (ZFC) magnetization measurements under an applied field of 50 Oe in the temperature range of 10–300 K were performed as warming up. The field-dependent magnetization measurements were conducted from −2.5 to 2.5 T at 10 and 300 K, respectively. The total mass with capping molecules was used for calculation. The dried pellet of the nanoparticles was scanned using Perkin Elmer Fourier Transform infrared (FT-IR) Spectrometer from 400 to 4000 cm^{-1} with a resolution of 4 cm^{-1} for 64 scans. The XPS measurements were carried out using a ScientaOmicron ESCA 2SR X-ray Photoelectron Spectroscope System equipped with a flood source neutralizer. Samples were loaded into the loadlock and pumped until the vacuum was below 5×10^{-7} mBar before they were transferred into the sample analysis chamber. All analyses were carried out with a Mono Al Kα X-ray source (1486.6 eV) at the power of 450 W, and the pressure in the analysis chamber was maintained below 3×10^{-9} mbar. Both a survey scan and high-resolution core level region scan of each element for all samples were recorded and calibrated with the C–C bond of C 1s peak at 284.8 eV. The core level spectra were also deconvoluted to obtain chemical state information. The atomic percentages were calculated based on the integrated area of each element. The sensitivity factor of each element was taken into consideration. T_1 and T_2 relaxation times of a series of nanoparticles in water dispersion of different iron concentrations were measured by Niumag 0.5 T relaxometer at 32 °C with parameters of SF, 18 MHz; TW, 8000 ms; SW, 200 kHz; RG, 20 db; DRG1, 3. NMR Analyzing Software Ver. 4.0 was used to compute for T_1 and T_2. The specific relaxivities of r_1 and r_2 for each nanoparticle were computed by taking the linear slope of $1/T_1$ (or $1/T_2$) versus Fe concentration. T_1- and T_2-weighted phantom images were acquired with a spin-echo (SE) sequence: TR/TE = 500/20 ms (T_1), TR/

TE = 5000/100 ms (T_2), matrices = 128 × 128, thickness = 0.8 mm, slice = 1. The iron concentration was analyzed with an inductively coupled plasma mass spectrometer (ICP-MS) (Varian 820).

3. Results and discussions

3.1. Synthesis of water-dispersible nanoparticles in different temperatures.

To study the temperature effect on the iron oxide nanoparticles synthesis, we synthesized iron oxide nanoparticles at different reaction temperatures using the continuous growth method [21]. The decomposition temperature of $Fe(acac)_3$ is 186 °C [33]. At the reaction temperature of 190 °C, the nanoparticles start to form. The sizes of nanoparticles are 3.0 ± 0.8, 4.8 ± 0.9, and 5.7 ± 0.8 nm for three continuous growth (Fig. 1a, b, c). The size of nanoparticles increases as the precursors are added, which is consistent with the previously reported work [21,34]. When the temperature is raised to 220 °C, the sizes of iron oxide nanoparticles are 4.4 ± 0.6, 7.1 ± 1.0, and 8.6 ± 1.4 nm respectively, increasing as we add precursors to three consecutive growth (Fig. 1d, e, & f). The sizes are 5.3 ± 0.9, 7.4 ± 1.2, and 10.9 ± 1.6 nm as the temperature is increased to 235 °C (Fig. 1g, h, & i). At each consecutive growth, we observe that the size is obviously larger at a higher reaction temperature. The plots of the corresponding particle size distribution (PSD) confirm that the size increase with the addition of precursor and the size distributions are narrow (Fig. S1). The increase of size at higher temperatures is probably due to the higher growth rate. As described in the classical Lamer mechanism for nanoparticle synthesis, higher temperature led to a higher nucleation rate [35]. As a result, a relatively less amount of nanoparticle seeds is generated at a higher temperature. A larger size will be produced with the same amount of precursor.

To exclude the time effect on the synthesis of iron oxide nanoparticles, we studied the size in a prolonged time of 6 h without the addition of precursor at different temperatures. According to XRD (Fig. S2), the nanoparticles can form after 0.5 h, and the diffraction peaks are constant after 2 h. The result demonstrates that the size of nanoparticles will not change after 2 h if no precursor is added at different temperatures.

Often time high reaction temperature was employed to achieve high efficiency growth. A boiling point is commonly utilized to synthesize iron oxide nanoparticles because the temperature can be easily controlled. Interestingly, when the temperature is raised further to the boiling point of DEG (245 °C), we observe the precipitate during the reaction (Fig. 2a). The nanoparticles do not disperse well in water after purification and precipitate immediately (Fig. 2b). In addition, we find the aggregate of nanoparticles under TEM (Fig. 2c).

As a comparison, all nanoparticles from three-consecutive growth at 190, 220, and 235 °C exhibit excellent dispersibility in the aqueous solution for up to 30 days (Fig. 3a, b & c). In a previous study, we showed that the surface ligands on the nanoparticles were DEG which rendered the high colloidal stability of nanoparticles in aqueous solution as evidenced by zeta potential, FTIR, XPS, and TGA measurements [21].

The aggregation of nanoparticles at reflux temperature is likely because the higher reaction temperature leads to uncontrolled fast nucleation and growth of nanoparticles. In addition, the DEG ligands on the surface may be stripped off and induce the aggregation of nanoparticles [36]. The result may explain the unsuccessful synthesis of iron oxide nanoparticles in polyols with the aggregation in previous studies [15,32]. We will further explore the possible mechanism for the precipitation below.

3.2. Surface properties

To explain the low water stability of iron oxide nanoparticles at high temperatures, we studied the surface properties of nanoparticles synthesized at 190, 235 °C, and boiling point (245 °C). The XPS peak deconvolution of Fe 2p, O 1s, and C 1s is compared. In general, Fe 2p can be fitted into Fe $2p_{1/2}$ (~723 eV) and Fe $2p_{3/2}$ (~710 eV) envelope,

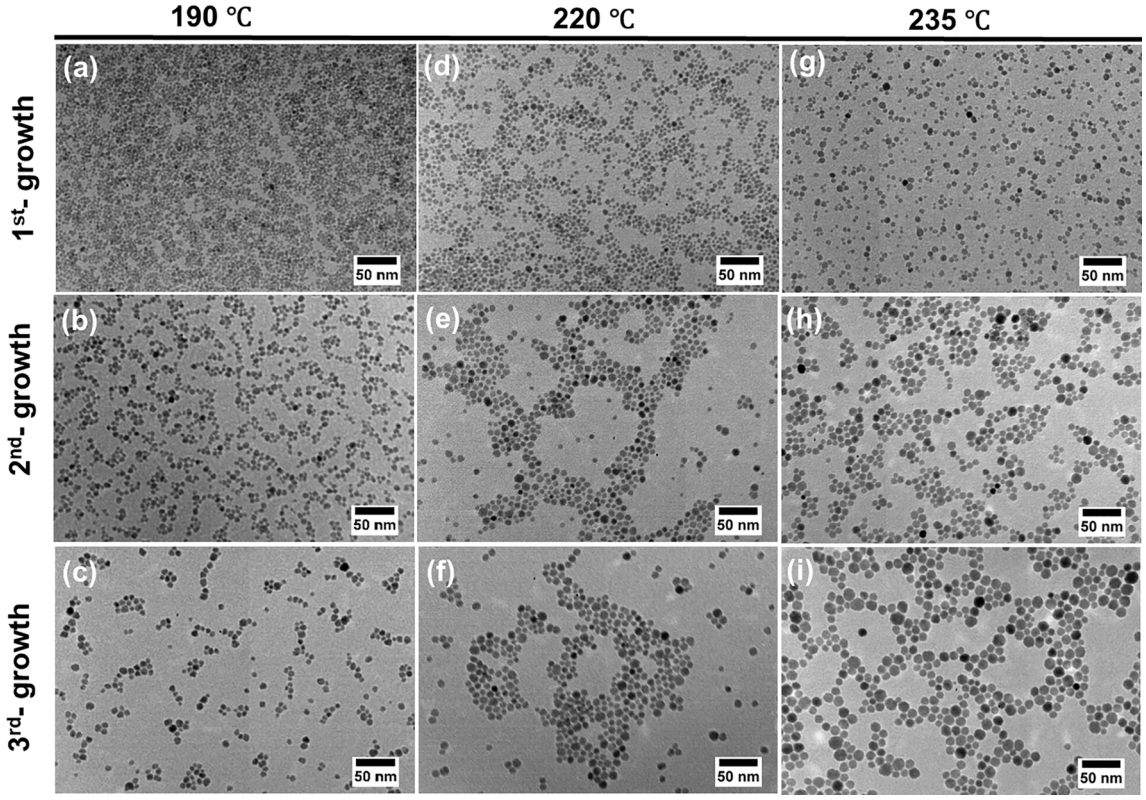

Fig. 1. TEM images of nanoparticles with three consecutive growth at 190 °C (a, b, & c), 220 °C (d, e, & f), and 235 °C (g, h, & i). The scale bar is 50 nm.

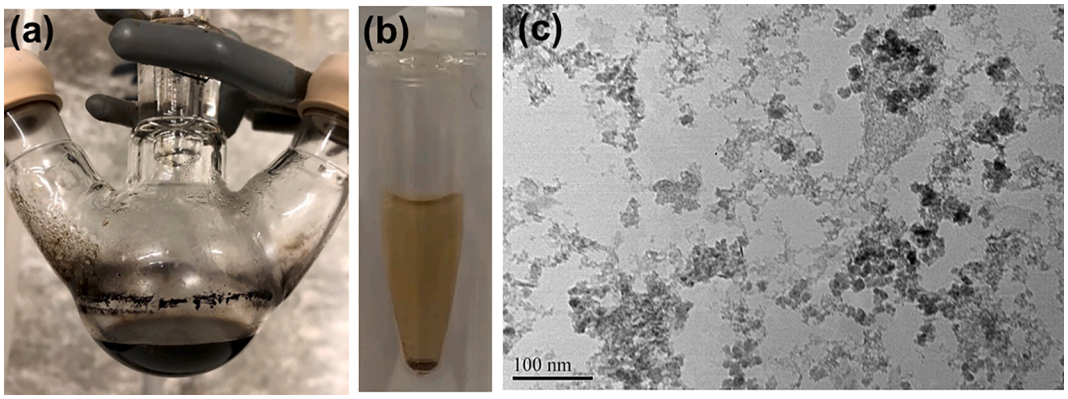

Fig. 2. The synthesis of iron oxide nanoparticles at the boiling point of diethylene glycol (245 °C): (a) Photographs showing nanoparticles attached to the wall of the reaction flask; (b) the instant precipitation of nanoparticles in water dispersion after purification, and (c) TEM of nanoparticles synthesized at reflux temperature.

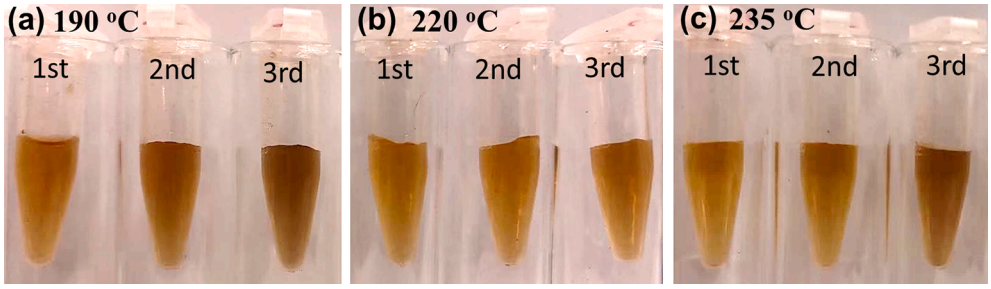

Fig. 3. Photographs of nanoparticles dispersion in water (after 30 days) for three consecutive growth nanoparticles synthesized at (a) 190 °C, (b) 220 °C, and (c) 235 °C.

confirming the presence of Fe^{2+} and Fe^{3+} in the magnetite (Fe_3O_4) phase (Fig. 4a, d, and g) [21,37–40]. High resolution O 1s spectrum is well fitted into 3 peaks for lattice oxygen of Fe-O in magnetite Fe_3O_4 at ~529 eV, monodentate oxygen moiety (C-O) at ~530 eV, and bidentate carboxylate moiety (O=C-O) at ~532 eV (Fig. 4b, e, and h) [39,41]. In the C 1s spectrum (Fig. 4c, f, and i), we assign the peaks for alkyl carbon bond (C–C) at 284.7 eV, (C-O) at 285.4 eV and the carboxylate moiety (O-C=O) at 287.5 eV [41,42]. Detailed analysis of O 1s and C 1s and corresponding peaks are listed in Table S1.

In the wide scan survey (Fig. 5a), we notice a relatively high carbon peak for iron oxide nanoparticles prepared at boiling points (245 °C) comparing to those synthesized at 190 and 235 °C. The atomic ratios (O/Fe, C/Fe, and O/C) of these samples are calculated according to the integrated area of corresponding peaks from high resolution spectra. As shown in Fig. 5b, the elemental composition shows no obvious difference between the nanoparticles synthesized at 190 and 235 °C, while the precipitates obtained at reflux temperature exhibit significantly high hydrocarbon (C and O).

FTIR for iron oxide nanoparticles synthesized at 190 °C and 235 °C present the similar characteristic peaks at 1060 cm^{-1}, 1120 cm^{-1} and 2950 cm^{-1} attributed to C-O and C–H vibration of DEG (Fig. 5c) [43,44]. The broad absorption at 3150 cm^{-1} corresponds to the O–H stretching from both DEG and adsorbed water. Strong absorption peak at 550 cm^{-1} is contributed by the Fe-O vibration [45]. Carboxylate groups are presented at 1430 cm^{-1} and 1616 cm^{-1} corresponding to symmetric and asymmetric COO– stretching [37,46,47]. Iron oxide nanoparticles synthesized at reflux (245 °C) samples on the other hand gives very strong and defined C–H at 3070 cm^{-1} and 2950 cm^{-1}, while Fe-O peak is greatly diminished. This indicated that there is an increase of hydrocarbon content in the reflux samples which is consistent with the XPS results.

Previously, metallic iron passivated in tetraethylene glycol was reported to have high hydrocarbon content and loss of functionality from the XPS spectra, indicating the thermal degradation of polyol during the passivation reaction [48]. Costa et al. proposed that metal complex with the oxygen atoms of the polyethylene oxide backbone weakened the C-O bond and reduced its thermal stability in a nitrogen environment [49]. As for our case, the reaction of iron precursors in DEG solvent at very high temperature such as reflux temperature may cause DEG to degrade into oxidized organic species (high hydrocarbon content). The DEG on the surface might lose the stabilizing capability and result in precipitation and aggregation.

3.3. The crystal structure of iron oxide nanoparticles.

The X-ray diffraction (XRD) patterns are measured for the nanoparticles prepared from three consecutive growth at 190, 220, and 235 °C (Fig. 6). The XRD patterns of all nanoparticles are indexed as the standard bulk phase of the spinel iron oxide structure [27,37,50,51]. With increasing reaction temperature at each consecutive growth, the peaks of XRD become sharper and more intense, which implies the increase in nanoparticles size or growth of the crystal grain. The maghemite (γ-Fe_2O_3) and magnetite (Fe_3O_4) are difficult to elucidate with XRD in our case as both have only a subtle difference.

Crystallite size (D_p) calculated by the Debye-Scherrer equation further confirms the size growth with increasing temperature at each consecutive growth. At all temperatures, the calculated D_p sizes are very close to those measured by TEM for each corresponding nanoparticle (Table S2). The results indicate that the nanoparticles are made from single domains, consistent with a continuous growth mechanism.

3.4. Magnetization property

We studied the effect of synthetic temperature on magnetic properties. To comparison, the nanoparticles with a similar size (~5 nm) synthesized at 190 °C (4.8 ± 0.9 nm) and 235 °C (4.5 ± 0.7 nm) were

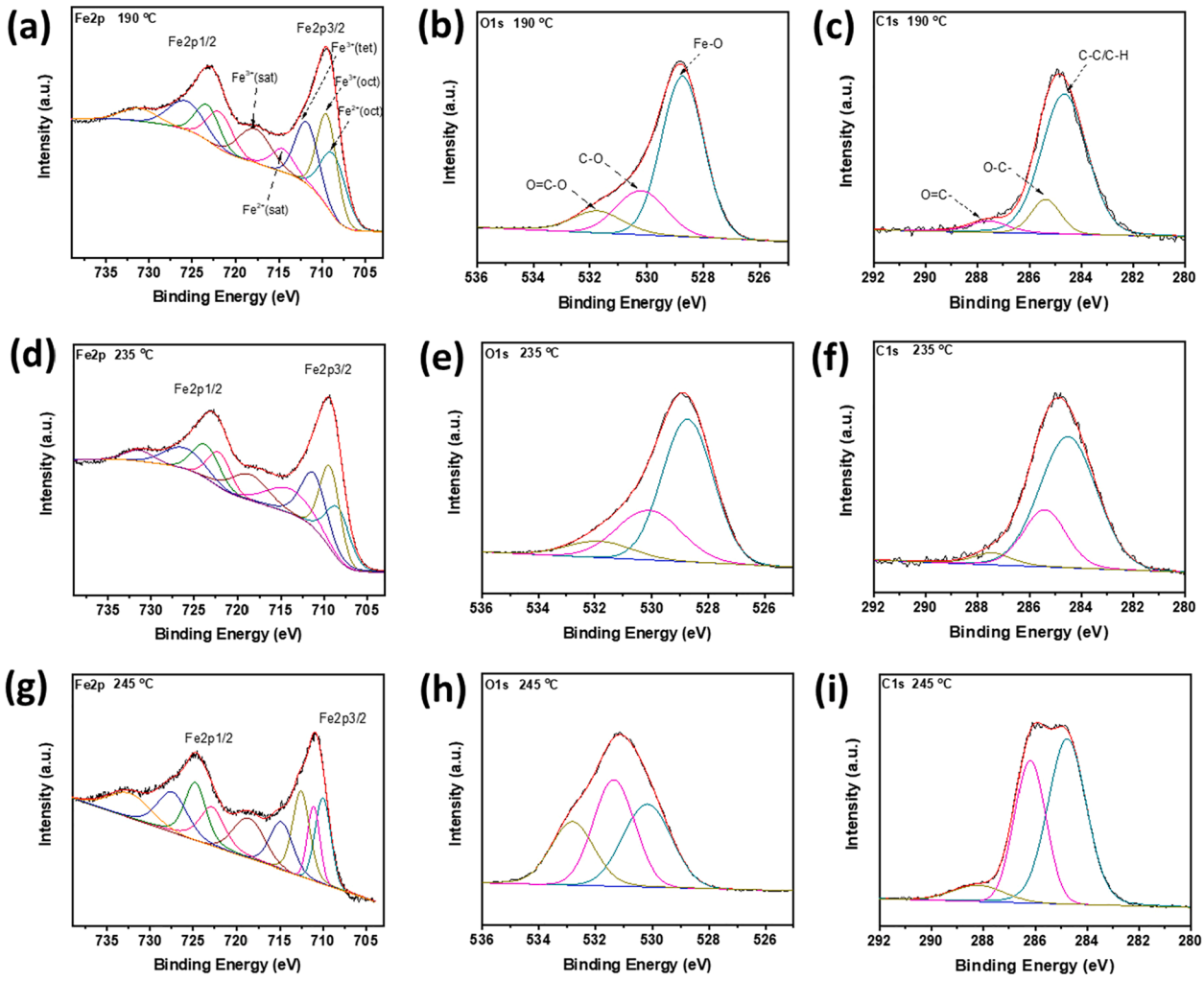

Fig. 4. XPS (Fe 2p, O 1s, and C 1s) for 5 nm nanoparticles synthesized at (a, b, & c) 190 °C, (d, e, & f) 235 °C, and (g, h, & i) precipitate obtained from reflux (245 °C).

studied. At 300 K, both nanoparticles exhibit superparamagnetic behavior with no remanence or coercivity observed in the hysteresis loops (Fig. 7a). The saturation magnetizations (M_s) for these nanoparticles at 300 K are 53.6 and 55.3 emu/g for nanoparticles synthesized at 190 and 235 °C, respectively. These M_s values are very close to the reported value of 51 emu/g for ~5 nm magnetite nanoparticles prepared by thermal decomposition of $Fe(acac)_3$ in phenyl ether and oleylamine [28]. In the hysteresis loops at 10 K, both nanoparticles display paramagnetic behavior with an estimated remanence of 10.3 emu/g and coercivity of 133.6 Oe (Fig. 7b). The M_s at 10 K is found to be 69.3 and 71.1 emu/g for nanoparticles synthesized at 190 and 235 °C, respectively. Although the size prepared at 190 °C is slightly higher, the saturate magnetism is slightly lower, indicating a better crystal structure at a higher temperature. It was reported that higher reaction temperature might form nanoparticles with higher crystallinity and result in a higher magnitude of M_s [28]. In this study, the difference in magnetic property is small. The magnetic properties are almost the same as long as the size is close. It is noted that the nanoparticles synthesized at 190 °C are obtained from the second growth, and the nanoparticles at 235 °C are from the first growth. The magnetic property implies the unique reaction mechanism of continuous growth in polyols. A high crystallinity is obtained at a lower temperature, which is comparable to a high temperature. The reaction temperature, size, and saturation magnetization (M_s) are summarized in Table S3.

3.5. Magnetic resonance properties of iron oxide nanoparticles synthesized at different temperatures.

In order to demonstrate the ability to customize these nanoparticles as the MRI contrast agents, we measured the longitudinal relaxivity (r_1) and transverse relaxivity (r_2) at 0.5 T. The inverses of relaxation times ($1/T_1$ or $1/T_2$) are plotted against different iron concentrations. As shown in the typical plots for nanoparticles prepared at 235 °C, a linear relationship is derived. (Fig. 8a and Fig. 8b). The relaxivities (r_1 or r_2) are calculated from the slopes.

MR phantom images demonstrate that the nanoparticles can be used as both T_1 and T_2 contrast agents. The typical T_2-weighed MR phantom images of the nanoparticles with different sizes are shown in Fig. 8c. The nanoparticles are efficient T_2-weighed contrast agents as the images of the nanoparticles tend to be darker with increasing iron concentration. In addition, the larger nanoparticles exhibit a more significant reduction in T_2 relaxation time. As displayed in Fig. 8d, the T_1-weighed MR images of the samples tend to be brighter with increasing iron concentration, indicating that the nanoparticles as positive contrast agents can effectively reduce the spin–lattice relaxation time of water protons. Furthermore, small-sized nanoparticles exhibited a more significant reduction in T_1 relaxation time, as shown by the much brighter images at the designated Fe concentrations.

The r_1 and r_2 of nanoparticles from continuous growth at different temperatures are calculated (Table 1). At a given temperature, the r_1 and r_2 increase with continuous growth from the first growth to the third

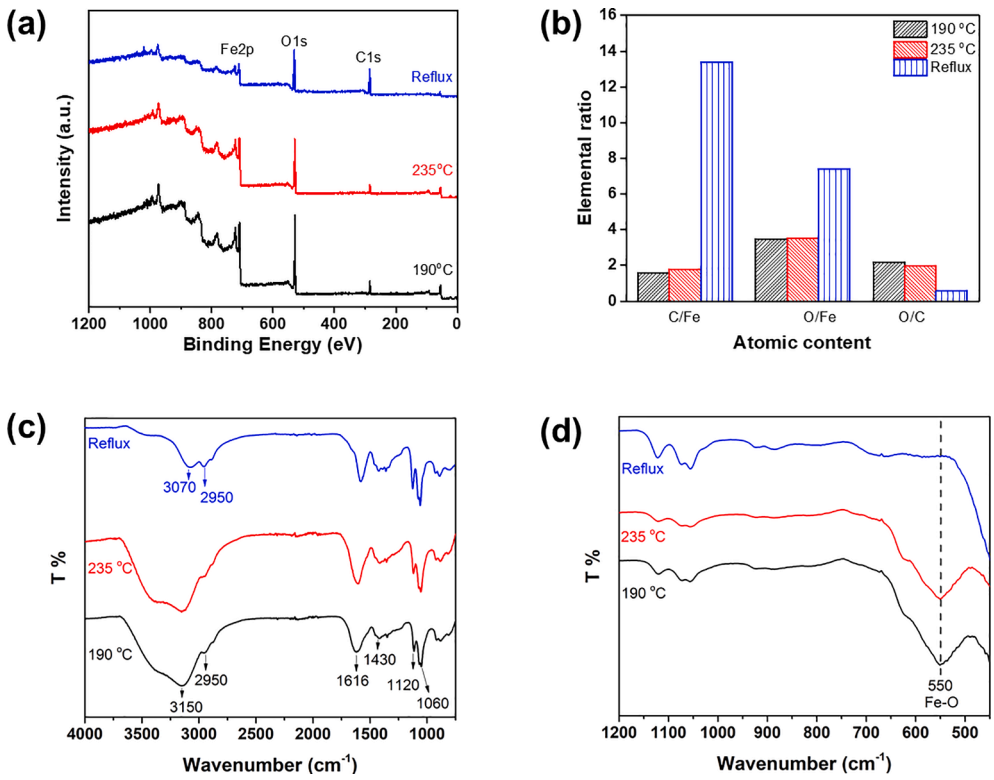

Fig. 5. XPS for a) wide scan, b) atomic ratio, c) FTIR (4000–750 cm^{-1}), and d) FTIR (1200–450 cm^{-1}) for 5 nm nanoparticles synthesized at 190 °C, 235 °C, and precipitate obtained from reflux (245 °C).

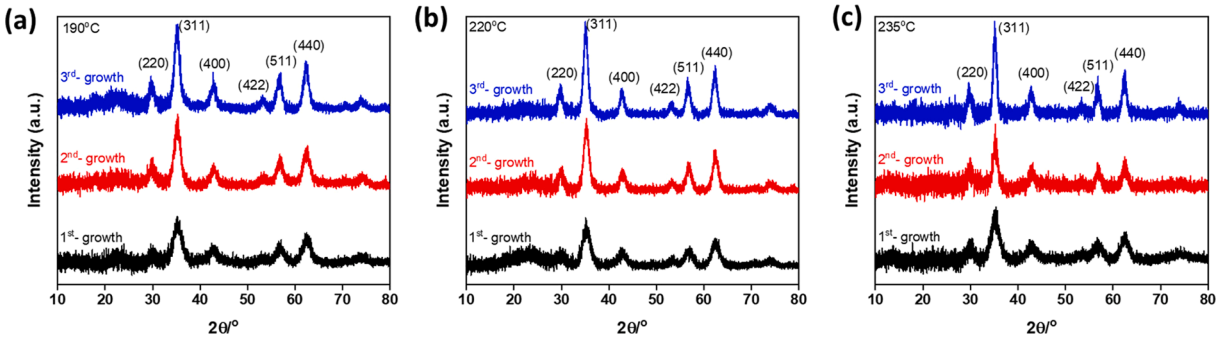

Fig. 6. XRD patterns for three consecutive growth nanoparticles synthesized at (a) 190 °C, (b) 220 °C, and (c) 235 °C.

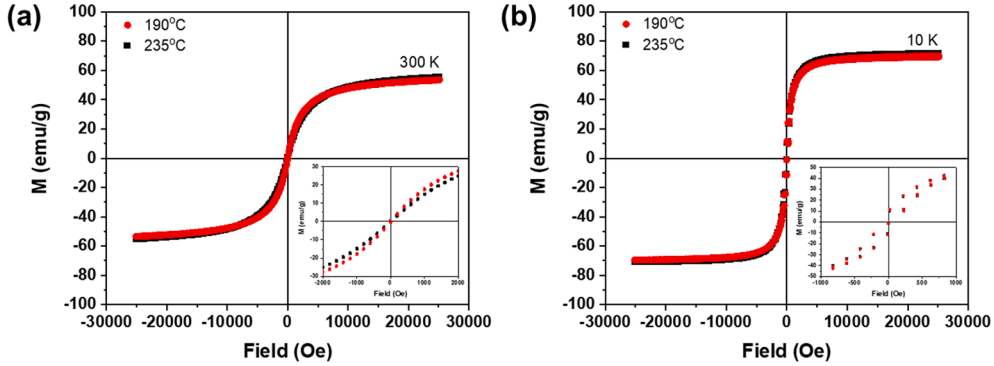

Fig. 7. Magnetization as a function of the magnetic field measured at (a) 300 K, (b) 10 K for 5 nm iron oxide nanoparticles synthesized at 190 °C and 235 °C.

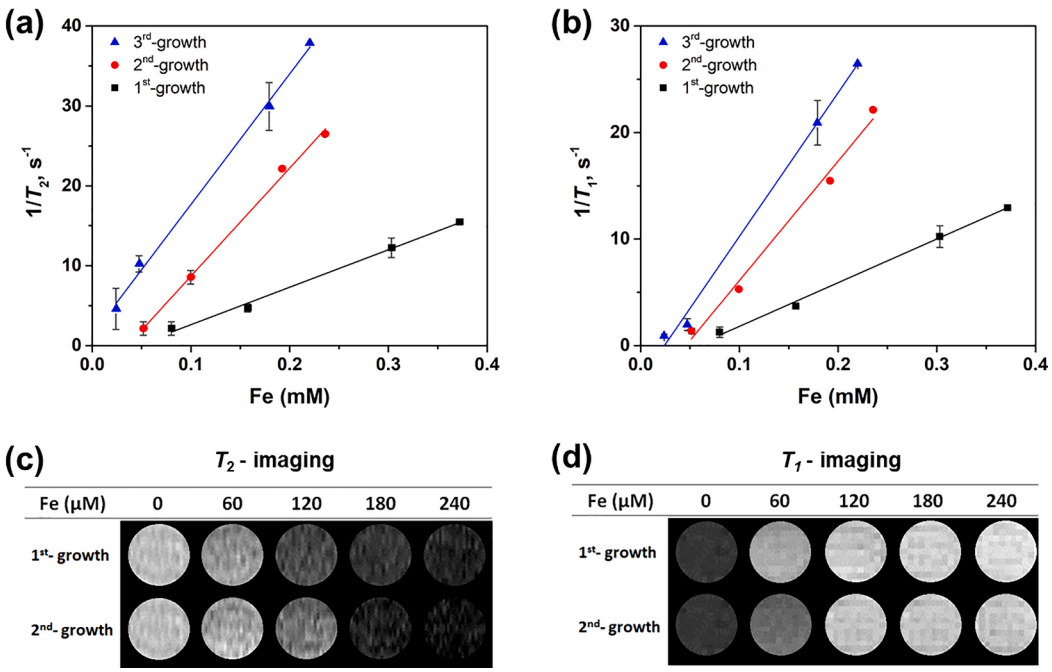

Fig. 8. (a) The inverse of T_2-weighed and (b) T_1-weighed relaxation times as the function of iron concentrations; (c) T_2-weighed and (d) T_1-weighed MR phantom images for nanoparticles synthesized at 235 °C.

Table 1
Summary of r_2, r_1, and r_2/r_1 of nanoparticles from three consecutive growth synthesized at 190 °C, 220 °C, and 235 °C.

		r_2, $mM^{-1}s^{-1}$	r_1, $mM^{-1}s^{-1}$	r_2/r_1
1st growth	190 °C	18.9	16.8	1.12
	220 °C	30.9	28.1	1.10
	235 °C	46.9	41.0	1.14
2nd growth	190 °C	52.1	49.5	1.05
	220 °C	90.6	78.3	1.16
	235 °C	135.4	112.2	1.21
3rd growth	190 °C	78.3	76.2	1.03
	220 °C	145.5	132.3	1.10
	235 °C	163.4	135.0	1.21

growth. With the increase of reaction temperature, a higher r_2 or r_1 value will be obtained at the same consecutive growth stage, which is consistent with the size growth as measured by the TEM and XRD (Table S2). For example, the third consecutive growth of nanoparticles at 235 °C produced nanoparticles with size 10.9 ± 1.6 nm, reported to have relatively high relaxivities with r_2 of 163.4 $mM^{-1}s^{-1}$ and r_1 of 135.0 $mM^{-1}s^{-1}$. There are many studies on the relationship between nanoparticle size and relaxivities (r_2 and r_1) [19,52,53]. The well correlation of size and relaxivity in this study demonstrates that the continuous growth at different temperatures can be used to tune the size and relaxivities precisely according to different applications. The MR contrast agent with enhanced r_2 or r_1 values can greatly improve the sensitivity.

4. Conclusions

In conclusion, we studied the essential role of the reaction temperature in the continuous growth of water-dispersible iron oxide nanoparticles in DEG. The nanoparticles are highly water dispersible when the reaction temperatures are 190, 220, and 235 °C. Larger nanoparticles can be obtained with the increase of the temperature. However, the synthesis of iron oxide nanoparticles at reflux temperature (245 °C) results in aggregations and precipitation. The XPS and FTIR analysis reveals that nanoparticle precipitation is associated with high carbon concentration, which may indicate the decomposition of DEG. This study shows that size-controlled water-dispersible iron oxide nanoparticles can be prepared by the continuous growth method if the temperatures are controlled at 235 °C and below. The result provides insight into why aggregation was observed in literature for polyols synthesis. The nanoparticles consist of a single-grain domain as shown in TEM and XRD. The crystal structure of the nanoparticles exhibits a magnetite phase. The magnetic properties are largely affected by size, which can be tuned by the reaction temperature. The relaxivity properties are well correlated with the size of nanoparticles prepared at various temperatures. This work demonstrated the possibility of tuning the physicochemical properties of iron oxide nanoparticles for specific applications via the reaction temperatures of continuous growth in DEG.

CRediT authorship contribution statement

Pohlee Cheah: Conceptualization; Formal analysis; Investigation; Writing - original draft. **Jing Qu:** Formal analysis; Investigation. **Yu Li:** Formal analysis; Investigation. **Dongmei Cao:** Formal analysis; Investigation. **Xianchun Zhu:** Formal analysis; Investigation. **Yongfeng Zhao:** Conceptualization; Formal analysis; Writing - review & editing.

Declaration of Competing Interest

The authors declare that they have no known competing financial interests or personal relationships that could have appeared to influence the work reported in this paper.

Acknowledgement

This research was supported by the National Science Foundation (grant number: HRD-1700390, DMR-2000135) and NSF EPSCoR (grant number: OIA-1757220).

Appendix A. Supplementary data

Supplementary data to this article can be found online at https://doi.

org/10.1016/j.jmmm.2021.168481.

References

[1] N. Lee, D. Yoo, D. Ling, M.H. Cho, T. Hyeon, J. Cheon, Iron oxide based nanoparticles for multimodal imaging and magnetoresponsive therapy, Chem. Rev. 115 (2015) 10637–10689.

[2] S. Laurent, D. Forge, M. Port, A. Roch, C. Robic, L. Vander Elst, R.N. Muller, Magnetic iron oxide nanoparticles: synthesis, stabilization, vectorization, physicochemical characterizations, and biological applications, Chem. Rev. 108 (2008) 2064–2110.

[3] S. Tong, C.A. Quinto, L. Zhang, P. Mohindra, G. Bao, Size-dependent heating of magnetic iron oxide nanoparticles, ACS Nano 11 (2017) 6808–6816.

[4] Y. Bao, J.A. Sherwood, Z. Sun, Magnetic iron oxide nanoparticles as T1 contrast agents for magnetic resonance imaging, J. Mater. Chem. C 6 (2018) 1280–1290.

[5] V. Trujillo-Alonso, E.C. Pratt, H. Zong, A. Lara-Martinez, C. Kaittanis, M.O. Rabie, V. Longo, M.W. Becker, G.J. Roboz, J. Grimm, M.L. Guzman, FDA-approved ferumoxytol displays anti-leukaemia efficacy against cells with low ferroportin levels, Nat. Nanotechnol. 14 (2019) 616–622.

[6] R. Massart, Preparation of aqueous magnetic liquids in alkaline and acidic media, IEEE Trans. Magn. 17 (2) (1981) 1247–1248.

[7] R.Y. Hong, T.T. Pan, Y.P. Han, H.Z. Li, J. Ding, S. Han, Magnetic field synthesis of Fe3O4 nanoparticles used as a precursor of ferrofluids, J. Magn. Magn. Mater. 310 (2007) 37–47.

[8] K.S. Suslick, S.-B. Choe, A.A. Cichowlas, M.W. Grinstaff, Sonochemical synthesis of amorphous iron, Nature 353 (1991) 414–416.

[9] R. Abu-Much, U. Meridor, A. Frydman, A. Gedanken, Formation of a three-dimensional microstructure of Fe3O4−poly(vinyl alcohol) composite by evaporating the hydrosol under a magnetic field, J. Phys. Chem. B 110 (2006) 8194–8203.

[10] K. Eun Hee, L. Hyo Sook, K. Byung Kook, K. Byung-Kee, Synthesis of ferrofluid with magnetic nanoparticles by sonochemical method for MRI contrast agent, J. Magn. Magn. Mater. 289 (2005) 328–330.

[11] M.H. Maen, N.N. Nashaat, Nanoparticle preparation using the single microemulsions scheme. Curr. Nanosci. 4 (2008) 370–380.

[12] S. Ge, X. Shi, K. Sun, C. Li, C. Uher, J.R. Baker, M.M. Banaszak Holl, B.G. Orr, Facile hydrothermal synthesis of iron oxide nanoparticles with tunable magnetic properties, J. Phys. Chem. C 113 (2009) 13593–13599.

[13] H. Cai, X. An, J. Cui, J. Li, S. Wen, K. Li, M. Shen, L. Zheng, G. Zhang, X. Shi, Facile hydrothermal synthesis and surface functionalization of polyethyleneimine-coated iron oxide nanoparticles for biomedical applications, ACS Appl. Mater. Interfaces 5 (2013) 1722–1731.

[14] Y.B. Khollam, S.R. Dhage, H.S. Potdar, S.B. Deshpande, P.P. Bakare, S.D. Kulkarni, S.K. Date, Microwave hydrothermal preparation of submicron-sized spherical magnetite (Fe3O4) powders, Mater. Lett. 56 (2002) 571–577.

[15] W. Cai, J. Wan, Facile synthesis of superparamagnetic magnetite nanoparticles in liquid polyols, J. Colloid Interface Sci. 305 (2) (2007) 366–370.

[16] M. Vázquez, C. Luna, M.P. Morales, R. Sanz, C.J. Serna, C. Mijangos, Magnetic nanoparticles: synthesis, ordering and properties, Physica B 354 (2004) 71–79.

[17] S. Sun, H. Zeng, Size-controlled synthesis of magnetite nanoparticles, J. Am. Chem. Soc. 124 (28) (2002) 8204–8205.

[18] J.-H. Lee, Y.-M. Huh, Y.-W. Jun, J.-W. Seo, J.-T. Jang, H.-T. Song, S. Kim, E.-J. Cho, H.-G. Yoon, J.-S. Suh, J. Cheon, Artificially engineered magnetic nanoparticles for ultra-sensitive molecular imaging, Nat. Med. 13 (2007) 95–99.

[19] B.H. Kim, N. Lee, H. Kim, K. An, Y.I. Park, Y. Choi, K. Shin, Y. Lee, S.G. Kwon, H. B. Na, J.-G. Park, T.-Y. Ahn, Y.-W. Kim, W.K. Moon, S.H. Choi, T. Hyeon, Large-scale synthesis of uniform and extremely small-sized iron oxide nanoparticles for high-resolution T1 magnetic resonance imaging contrast agents, J. Am. Chem. Soc. 133 (2011) 12624–12631.

[20] Y. Xu, Y. Qin, S. Palchoudhury, Y. Bao, Water-soluble iron oxide nanoparticles with high stability and selective surface functionality, Langmuir 27 (2011) 8990–8997.

[21] P. Cheah, T. Cowan, R. Zhang, A. Fatemi-Ardekani, Y. Liu, J. Zheng, F. Han, Y. Li, D. Cao, Y. Zhao, Continuous growth phenomenon for direct synthesis of monodisperse water-soluble iron oxide nanoparticles with extraordinarily high relaxivity, Nanoscale 12 (2020) 9272–9283.

[22] T. Theppaleak, G. Tumcharern, U. Wichai, M. Rutnakornpituk, Synthesis of water dispersible magnetite nanoparticles in the presence of hydrophilic polymers, Polym. Bull. 63 (2009) 79–90.

[23] Z. Li, H. Chen, H. Bao, M. Gao, One-pot reaction to synthesize water-soluble magnetite nanocrystals, Chem. Mater. 16 (2004) 1391–1393.

[24] F. Zhao, B. Zhang, L. Feng, Preparation and magnetic properties of magnetite nanoparticles, Mater. Lett. 68 (2012) 112–114.

[25] J. Wang, B. Zhang, L. Wang, M. Wang, F. Gao, One-pot synthesis of water-soluble superparamagnetic iron oxide nanoparticles and their MRI contrast effects in the mouse brains, Mater. Sci. Eng., C 48 (2015) 416–423.

[26] B. Zhang, Z. Tu, F. Zhao, J. Wang, Superparamagnetic iron oxide nanoparticles prepared by using an improved polyol method, Appl. Surf. Sci. 266 (2013) 375–379.

[27] J. Park, K. An, Y. Hwang, J.-G. Park, H.-J. Noh, J.-Y. Kim, J.-H. Park, N.-M. Hwang, T. Hyeon, Ultra-large-scale syntheses of monodisperse nanocrystals, Nat. Mater. 3 (2004) 891–895.

[28] D. Maity, J. Ding, J. Xue, Synthesis of magnetite nanoparticles by thermal decomposition: Time, temperature, surfactant and solvent effects, Funct. Mater. Lett. 01 (2008) 189–193.

[29] T. Iwamoto, T. Kinoshita, K. Takahashi, Growth mechanism and magnetic properties of magnetite nanoparticles during solution process, J. Solid State Chem. 237 (2016) 19–26.

[30] J.-H. Huang, H.J. Parab, R.-S. Liu, T.-C. Lai, M. Hsiao, C.-H. Chen, H.-S. Sheu, J.-M. Chen, D.-P. Tsai, Y.-K. Hwu, Investigation of the growth mechanism of iron oxide nanoparticles via a seed-mediated method and its cytotoxicity studies, J. Phys. Chem. C 112 (2008) 15684–15690.

[31] F.J. Douglas, D.A. MacLaren, M. Murrie, A study of the role of the solvent during magnetite nanoparticle synthesis: tuning size, shape and self-assembly, RSC Adv. 2 (2012) 8027–8035.

[32] R. Hachani, M. Lowdell, M. Birchall, A. Hervault, D. Mertz, S. Begin-Colin, N.T. K. Thanh, Polyol synthesis, functionalisation, and biocompatibility studies of superparamagnetic iron oxide nanoparticles as potential MRI contrast agents, Nanoscale 8 (2016) 3278–3287.

[33] J.V. Hoene, R.G. Charles, W.M. Hickam, Thermal decomposition of metal acetylacetonates: mass spectrometer studies, J. Phys. Chem. 62 (1958) 1098–1101.

[34] P. Cheah, P. Brown, J. Qu, B. Tian, D.L. Patton, Y. Zhao, Versatile surface functionalization of water-dispersible iron oxide nanoparticles with precisely controlled sizes, Langmuir 37 (2021) 1279–1287.

[35] V.K. LaMer, R.H. Dinegar, Theory, production and mechanism of formation of monodispersed hydrosols, J. Am. Chem. Soc. 72 (1950) 4847–4854.

[36] J. Fu, L. He, W. Xu, J. Zhuang, X. Yang, X. Zhang, M. Wu, Y. Yin, Formation of colloidal nanocrystal clusters of iron oxide by controlled ligand stripping, Chem. Commun. 52 (2016) 128–131.

[37] L.-H. Shen, J.-F. Bao, D. Wang, Y.-X. Wang, Z.-W. Chen, L. Ren, X. Zhou, X.-B. Ke, M. Chen, A.-Q. Yang, One-step synthesis of monodisperse, water-soluble ultra-small Fe3O4 nanoparticles for potential bio-application, Nanoscale 5 (2013) 2133–2141.

[38] D. Wilson, M.A. Langell, XPS analysis of oleylamine/oleic acid capped Fe3O4 nanoparticles as a function of temperature, Appl. Surf. Sci. 303 (2014) 6–13.

[39] C. Iacovita, R. Stiufiuc, T. Radu, A. Florea, G. Stiufiuc, A. Dutu, S. Mican, R. Tetean, C.M. Lucaciu, Polyethylene glycol-mediated synthesis of cubic iron oxide nanoparticles with high heating power, Nanoscale Res. Lett. 10 (2015) 391.

[40] T. Fujii, F.M.F. de Groot, G.A. Sawatzky, F.C. Voogt, T. Hibma, K. Okada, In situ XPS analysis of various iron oxide films grown by ${\mathrm{NO}}_{2}$-assisted molecular-beam epitaxy, Phys. Rev. B 59 (1999) 3195–3202.

[41] J.F. Moulder, J. Chastain, Handbook of X-ray Photoelectron Spectroscopy: A Reference Book of Standard Spectra for Identification and Interpretation of XPS Data; Physical Electronics Division, Perkin-Elmer Corporation, 1992.

[42] S. Mondini, S. Cenedese, G. Marinoni, G. Molteni, N. Santo, C.L. Bianchi, A. Ponti, One-step synthesis and functionalization of hydroxyl-decorated magnetite nanoparticles, J. Colloid Interface Sci. 322 (2008) 173–179.

[43] F. Hu, K.W. MacRenaris, E.A. Waters, T. Liang, E.A. Schultz-Sikma, A. L. Eckermann, T.J. Meade, Ultrasmall, water-soluble magnetite nanoparticles with high relaxivity for magnetic resonance imaging, J. Phys. Chem. C 113 (2009) 20855–20860.

[44] S. Khoee, A. Kavand, A new procedure for preparation of polyethylene glycol-grafted magnetic iron oxide nanoparticles, J. Nanostruct. Chem. 4 (2014) 111.

[45] D. Maity, S.N. Kale, R. Kaul-Ghanekar, J.-M. Xue, J. Ding, Studies of magnetite nanoparticles synthesized by thermal decomposition of iron (III) acetylacetonate in tri(ethylene glycol), J. Magn. Magn. Mater. 321 (2009) 3093–3098.

[46] J. Ge, Y. Hu, M. Biasini, W. Beyermann, Y. Yin, Superparamagnetic magnetite colloidal nanocrystal clusters, Angew. Chem. Int. Ed. 46 (23) (2007) 4342–4345.

[47] R.H. Gonçalves, C.A. Cardoso, E.R. Leite, Synthesis of colloidal magnetite nanocrystals using high molecular weight solvent, J. Mater. Chem. 20 (2010) 1167–1172.

[48] E.d.S. Nunes, W.R. Viali, S.W. da Silva, J.A.H. Coaquira, V.K. Garg, A.C. de Oliveira, P.C. Morais, M. Jafelicci Júnior, Characterization of tetraethylene glycol passivated iron nanoparticles. Appl. Surf. Sci. 315 (2014) 337–345.

[49] L. Costa, A.M. Gad, G. Camino, G.G. Cameron, M.Y. Qureshi, Thermal and thermooxidative degradation of poly(ethylene oxide)-metal salt complexes, Macromolecules 25 (1992) 5512–5518.

[50] E.C. Vreeland, J. Watt, G.B. Schober, B.G. Hance, M.J. Austin, A.D. Price, B. D. Fellows, T.C. Monson, N.S. Hudak, L. Maldonado-Camargo, A.C. Bohorquez, C. Rinaldi, D.L. Huber, Enhanced nanoparticle size control by extending LaMer's mechanism, Chem. Mater. 27 (2015) 6059–6066.

[51] S.R. Cooper, L.K. Plummer, A.G. Cosby, P. Lenox, A. Jander, P. Dhagat, J. E. Hutchison, Insights into the magnetic properties of sub-10 nm iron oxide nanocrystals through the use of a continuous growth synthesis, Chem. Mater. 30 (2018) 6053–6062.

[52] H. Wei, O.T. Bruns, M.G. Kaul, E.C. Hansen, M. Barch, A. Wiśniowska, O. Chen, Y. Chen, N. Li, S. Okada, J.M. Cordero, M. Heine, C.T. Farrar, D.M. Montana, G. Adam, H. Ittrich, A. Jasanoff, P. Nielsen, M.G. Bawendi, Exceedingly small iron oxide nanoparticles as positive MRI contrast agents, Proc. Natl. Acad. Sci. U. S. A. 114 (2017) 2325–2330.

[53] J. Huang, L. Wang, X. Zhong, Y. Li, L. Yang, H. Mao, Facile non-hydrothermal synthesis of oligosaccharides coated sub-5 nm magnetic iron oxide nanoparticles with dual MRI contrast enhancement effect, J. Mater. Chem. B (2014).